Inhibition of Eco RV Endonuclease by Deoxyribo-3'- S -phosphorothiolates: A High-Resolution X-ray Crystallographic Study

3 AUTHORS, INCLUDING:

John Perona

Portland State University

90 PUBLICATIONS **3,493** CITATIONS

Inhibition of *Eco*RV Endonuclease by Deoxyribo-3′-*S*-phosphorothiolates: A High-Resolution X-ray Crystallographic Study

Nancy C. Horton,[†] Bernard A. Connolly,[‡] and John J. Perona*,[†]

Contribution from the Department of Chemistry and Biochemistry, and Interdepartmental Program in Biochemistry and Molecular Biology, University of California at Santa Barbara, Santa Barbara, California 93106-9510, and Department of Biochemistry and Genetics, The University of Newcastle, Newcastle upon Tyne NE2 4HH, United Kingdom

Received October 18, 1999

Abstract: Three high-resolution structures of the restriction endonuclease *Eco*RV bound to a duplex DNA substrate analogue with deoxyribo-3′-*S*-phosphorothiolate linkages at both scissile phosphates are presented. In each of these structures cocrystallized with Mg^{2+}, Mn^{2+}, or Ca^{2+} ions, the nonesterified *pro-S* oxygen of the scissile phosphate no longer directly ligates a divalent cation, as is observed for the unmodified complex. Instead, one metal ion in all three structures is shifted toward the adjacent 3′-phosphate of the DNA, to occupy a position nearly identical to that previously observed in an *Eco*RV T93A/DNA/Ca^{2+} complex (N. C. Horton et al., *Proc. Natl. Acad. Sci. U.S.A.* **1998**, *95*, 13489). A second divalent metal ion in each structure bridges the carboxylate groups of Asp74 and Glu45 (74/45 site), as also seen in both wild-type and T93A cocrystals. The uncleaved 3′-*S*-phosphorothiolate DNAs in these complexes are only slightly distorted from the conformation of the unmodified duplex. Kinetic measurements show that the rate of the chemical step for analogue cleavage is severely reduced for each of the active metals Mg^{2+}, Mn^{2+}, and Co^{2+}, and that the thiophilic Mn^{2+}, Cd^{2+}, and Zn^{2+} cations do not provide a measurable reconstitution of activity. The inability of thiophilic metals to improve activity is consistent with models for catalysis derived from previous crystal structures, which indicate that ligation of a metal ion to the 3′-oxygen is mediated through an inner-sphere water molecule rather than by direct interaction. The structures suggest that 3′-*S*-phosphorothiolate analogues resist cleavage because the bridging sulfur excludes inner-sphere ligation of divalent metal ions to any position on the scissile phosphate. This distinguishes the inhibitory mechanism in *Eco*RV from that operative in the 3′-5′ exonuclease active site of DNA polymerase I (C. A. Brautigam et al., *Biochemistry*, **1999**, *38*, 696), and likely as well from other enzymes which also catalyze phosphoryl transfer via direct metal ligation to the 3′-oxygen leaving group.

Introduction

*Eco*RV is an archetypical type II restriction endonuclease which cleaves duplex DNA at the center TA step of the target sequence GATATC, leaving blunt ends containing 5′-phosphate and 3′-OH groups.[1] As in all type II restriction enzymes, this phosphoryl transfer reaction requires divalent metal ions and involves attack of water or hydroxide ion on the scissile phosphate, resulting in inversion of configuration at phosphorus.[2] In vivo, the divalent cation cofactor is thought to be Mg^{2+} [3], but both Mn^{2+} and Co^{2+} also sustain catalysis at high levels in vitro.[4] Both the affinity and the sequence-specificity of DNA binding are enhanced by Ca^{2+}, which also functions as a potent inhibitor of catalysis.[5−7] The most critical active-site residues

have been identified by mutagenesis as Asp74, Asp90, and Lys92,[8] which form part of the motif P-E/D-X$_n$-E/D-Z-K (where Z is a hydrophobic residue) common to a subset of type II restriction endonucleases.[9]

The three-dimensional structure of *Eco*RV has been solved in the unliganded state[10,11] as well as in various binary and ternary complexes with divalent metal ions and cognate DNA,[11−14] nonspecific DNA,[12] DNA base-analogues,[15] and

* Corresponding author. Tel:805-893-7389; FAX: 805-893-4120.
† University of California at Santa Barbara.
‡ The University of Newcastle.
(1) Schildkraut, I.; Banner, C. D. B.; Rhodes, C. S.; Parekh, S. *Gene* **1984**, *27*, 327.
(2) (a) Connolly, B. A.; Eckstein, F.; Pingoud, A. *J. Biol. Chem.* **1984**, *259*, 10760. (b) Grasby, J. A.; Connolly, B. A. *Biochemistry* **1992**, *31*, 7855. (c) Mizuuchi, K.; Nobbs, T. J.; Halford, S. E.; Adzuma, K.; Qin, J. *Biochemistry* **1999**, *38*, 4640.
(3) Roberts, R. J.; Halford, S. E. In *Nucleases*, 2nd ed.; Linn, S. M., Lloyd, R. S., Roberts, R. J., Eds.; Cold Spring Harbor Laboratory Press: Plainview, NY, 1993; pp 35−88.
(4) Vipond, I. B.; Baldwin, G. S.; Halford, S. E. *Biochemistry* **1995**, *34*, 697.

(5) Vipond, I. B.; Halford, S. E. *Biochemistry* **1995**, *34*, 1113.
(6) Martin, A. M.; Horton, N. C.; Lusetti, S.; Reich, N. O.; Perona, J. J. *Biochemistry* **1999**, *38*, 8430.
(7) Engler, L. E.; Welch, K. K.; Jen-Jacobson, L. *J. Mol. Biol.* **1997**, *269*, 82.
(8) Selent, U.; Ruter, T.; Kohler, E.; Liedtke, M.; Thielking, V.; Alves, J.; Oelgeschager, T.; Wolfes, H.; Peters, F.; Pingoud, A. *Biochemistry* **1992**, *31*, 4808.
(9) (a) Thielking, V.; Selent, U.; Kohler, E.; Wolfes, H.; Pieper, U.; Geiger, R.; Urbanke, C.; Winkler, F. K.; Pingoud, A. *Biochemistry* **1991**, *30*, 6416. (b) Aggarwal, A. K. *Curr. Opin. Struct. Biol.* **1995**, *5*, 11.
(10) Winkler, F. K.; Banner, D. W.; Oefner, C.; Tsernoglou, D.; Brown, R. S.; Heathman, S. P.; Bryan, R. K.; Martin, P. D.; Petratos, K.; Wilson, K. S. *EMBO J.* **1993**, *12*, 1781.
(11) Perona, J. J.; Martin, A. M. *J. Mol. Biol.* **1997**, *273*, 207.
(12) Kostrewa, D.; Winkler, F. K. *Biochemistry* **1995**, *34*, 683.
(13) (a) Horton, N. C.; Perona, J. J. *J. Mol. Biol.* **1998**, *277*, 779. (b) Horton, N. C.; Perona, J. J. *J. Biol. Chem.* **1998**, *273*, 21721.
(14) Horton, N. C.; Newberry, K. J.; Perona, J. J. *Proc. Natl. Acad. Sci. U.S.A.* **1998**, *95*, 13489.

Inhibition of EcoRV Endonuclease

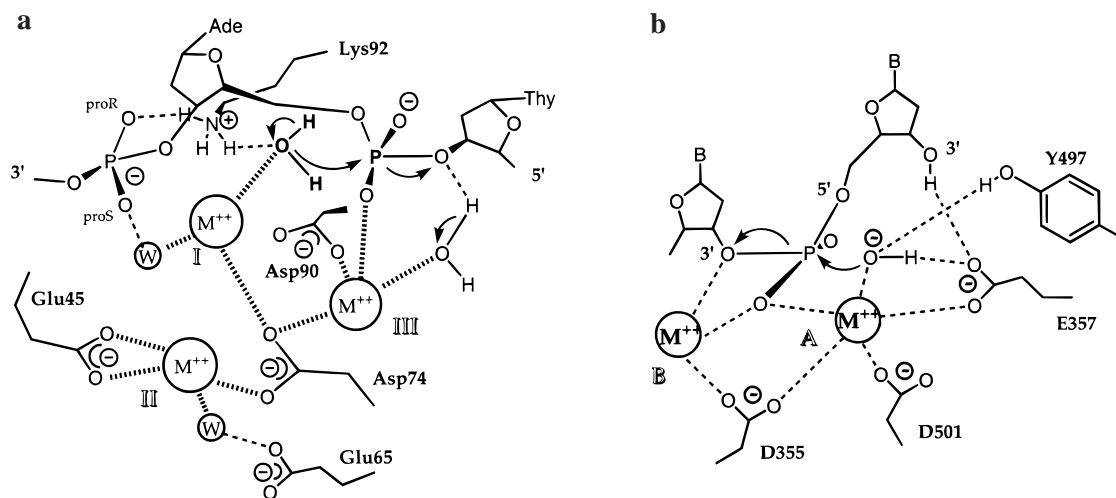*J. Am. Chem. Soc., Vol. 122, No. 14, 2000* 3315

Figure 1. (a) Model for the transition state of the metal-ion-mediated DNA cleavage by *Eco*RV, based on X-ray crystal structures of wild-type and T93A mutant enzymes[11,12,14] and consistent with biochemical data.[17,18,25,26] A metal ion located in site I generates the attacking hydroxide nucleophile, which is stabilized and oriented by the positively charged Lys92. The proton is released to solvent or associates transiently with a DNA phosphate or active-site carboxylate group. The site III metal stabilizes the incipient additional negative charge in the transition state and aids in water-mediated protonation of the leaving group. The site II metal plays a structural role. (b) Model for DNA hydroysis catalyzed by the 3′-5′ exonuclease active site of *E. coli* DNA polymerase I.[16a] Metal ion A generates the attacking hydroxide ion and stabilizes the incipient additional negative charge in the pentacovalent transition state, while metal B promotes the bond-breaking step by directly ligating the 3′-oxygen leaving group.

product DNA.[12] In each structure of the wild-type enzyme bound to divalent metal ions and specific DNA, one metal directly coordinates the *pro-S* oxygen of the scissile phosphate, bridging this group to the carboxylates of Asp90 and Asp74 (site III, Figure 1).[11,12] Each of the metals Mg^{2+}, Mn^{2+}, Co^{2+}, and Ca^{2+} is able to occupy this site.[11,12] In addition, a second metal ion has been located deeper in the active site between Asp74 and Glu45; in wild-type structures, this site (site II, Figure 1) can be filled by the active metals Mg^{2+}, Mn^{2+}, or Co^{2+}, but apparently not by the inactive Ca^{2+}.[11,12] The metal ion at this position does not directly ligate DNA.

The location of two metal ions in the active site suggested the possibility that *Eco*RV might function by a two-metal mechanism analogous to that proposed for alkaline phosphatase and for the 3′-5′ exonuclease activity of *Escherichia coli* DNA polymerase I.[16] In this mechanism, the attacking nucleophile originates as an inner-sphere water molecule bound to one metal, while the second metal ion stabilizes the pentacovalent transition state and facilitates leaving-group formation by directly ligating the 3′-oxygen. To accommodate this several proposals have been made suggesting a significant DNA rearrangement in the *Eco*RV active site prior to cleavage, to appropriately position the DNA relative to the metal ions bound in sites II and III.[4,12,17] An alternative mechanism is based on the finding of a distinct metal binding site on the phosphate group 3′ to the scissile phosphate in the *Eco*RV T93A mutant (site I).[14] The new metal site allows positioning of an inner-sphere water molecule in-line for attack. This led to a proposal for a three-metal substrate-assisted mechanism in which the DNA conformation observed in crystal structures is only slightly rearranged before reaching the transition state (Figure 1a).[14,18] While this has many similarities with the two-metal mechanism suggested for polymerase editing sites (Figure 1b),[16] an important distinction is that the leaving 3′-oxygen atom ligates a metal ion via a water-mediated rather

than a direct interaction. The observation of sharp bell-shaped pH-rate profiles for Mg^{2+}-dependent cleavage by *Eco*RV is consistent with a mechanism invoking the ionization of two inner-sphere water molecules in the catalytic event: the water bridging to the 3′-oxygen is proposed to protonate the leaving group.[18]

The introduction of a sulfur atom in place of oxygen at the 3′-leaving position yields 3′-phosphorothiolate (3′-PS) compounds, which have proven useful as mechanistic probes for enzymes which hydrolyze RNA or DNA.[19−21] In these experiments, the reconstitution of activity by substitution of Mg^{2+} with thiophilic cations such as Mn^{2+} or Cd^{2+} is interpreted to indicate inner-sphere ligation of the metal to the 3′-oxygen.[22] Crystal structures of the 3′-5′ exonuclease domain of *E. coli* DNA polymerase I (Klenow fragment) bound to 3′-PS-containing single-stranded DNA and divalent metal ions validated this interpretation, because thiophilic Mn^{2+} and Zn^{2+} ions were found to bind directly to the sulfur atom, whereas Mg^{2+} did not.[23] To date there has been no analysis of the structural effects of the 3′-PS analogue when present in both strands of duplex DNA.

Here we employ the 3′-PS substitution to evaluate the interaction of metal ions with the leaving oxygen atom in the DNA cleavage reaction catalyzed by *Eco*RV. *Eco*RV provides an interesting counterpoint to the study of Klenow fragment and other enzymes, since the suggested mechanism involves water-mediated rather than direct 3′-oxygen ligation by the metal ion. Further tests of this model for *Eco*RV catalysis are particularly important because it is derived by combining information from several different crystal structures.[14,18] An

(15) Martin, A. M.; Sam, M. D.; Reich, N. O.; Perona, J. J. *Nat. Struct. Biol.* **1999**, *6*, 269.

(16) (a) Beese, L. S.; Steitz, T. A. *EMBO J.* **1991**, *10*, 25. (b) Kim, E. E.; Wyckoff, H. W. *J. Mol. Biol.* **1991**, *218*, 449.

(17) Baldwin, G. S.; Sessions, R. B.; Erskine, S. G.; Halford, S. E. *J. Mol. Biol.* **1999**, *288*, 87.

(18) Sam, M. D.; Perona, J. J. *Biochemistry* **1999**, *38*, 6576.

(19) Vyle, J. S.; Connolly, B. A.; Kemp, D.; Cosstick, R. *Biochemistry* **1992**, *31*, 3012.

(20) Curley, J. F.; Joyce, C. M.; Piccirilli, J. A. *J. Am. Chem. Soc.* **1997**, *119*, 12691.

(21) (a) Piccirilli, J. A.; Vyle, J. S.; Caruthers, M. H.; Cech, T. R. *Nature* **1993**, *361*, 85. (b) Sontheimer, E. J.; Sun, S.; Piccirilli, J. A. *Nature* **1997**, *388*, 801. (c) Weinstein, L. B.; Jones, B. C. N. M.; Cosstick, R.; Cech, T. R. *Nature* **1997**, *388*, 805.

(22) Herschlag, D.; Piccirilli, J. A.; Cech, T. R. *Biochemistry* **1991**, *30*, 4844.

(23) Brautigam, C. A.; Sun, S.; Piccirilli, J. A.; Steitz, T. A. *Biochemistry* **1999**, *38*, 696.

3316 *J. Am. Chem. Soc., Vol. 122, No. 14, 2000*

Horton et al.

earlier study of 3′-PS cleavage by *Eco*RV, in the presence of the three metal ions Mg^{2+}, Mn^{2+}, and Co^{2+}, showed reductions in specific activity by at least 10^4-fold in each case.[19] The apparent inability of the thiophilic Mn^{2+} to improve cleavage rates indeed suggests the absence of an inner-sphere metal ion–3′-oxygen interaction. However, this conclusion requires closer examination, because the first-order rate constants for phosphoryl transfer were not measured and because a fuller range of thiophilic metals was not tested. Moreover, the lack of significant reconstitution by Mn^{2+} might well also be due to structural perturbations in the 3′-PS DNA–enzyme complex. That this could be the case was suggested by binding studies of the 3′-PS analogue with Mg^{2+} and Ca^{2+}.[7,24] It was found that Ca^{2+} and Mg^{2+} will stimulate binding by *Eco*RV to the 3′-PS substrate by 700-fold and 4-fold, respectively, in contrast to other studies of cleavable base-analogue substrates which indicated that the increase in binding affinity stimulated by either divalent cation is nearly equal.[6,15] This raises the possibility of metal ion-specific conformational differences in the 3′-PS DNA when bound in a ternary ground-state complex to *Eco*RV.

To explore the origins of catalytic inhibition by 3′-PS in the *Eco*RV system, we measured the first-order rate constants for phosphoryl transfer toward native and sulfur-substituted duplex DNA oligonucleotides containing the GATATC cleavage site, in the presence of Mg^{2+}, Mn^{2+}, Co^{2+}, Zn^{2+}, and Cd^{2+}. We find in all cases that the chemical step is reduced by at least 10^6-fold for cleavage of 3′-PS DNA (relative to Mg^{2+}-dependent rates on native substrates). None of the thiophilic cations Mn^{2+}, Cd^{2+}, or Zn^{2+} are able to reconstitute activity at detectable levels. Crystal structures of *Eco*RV bound to 3′-PS DNA and either Mg^{2+}, Mn^{2+}, or Ca^{2+} at 2.0, 1.9, and 1.6 Å resolution were then determined to characterize the structural effects of the sulfur substitution on the ground-state ternary complexes. The structures show that inhibition arises because the sulfur atom blocks inner-sphere ligation of a divalent cation to the nonesterified *pro-S* oxygen of the scissile phosphate group, so that the incipient negative charge acquired in the approach to the pentacovalent transition state is not neutralized. The implications of these findings for the catalytic pathway of *Eco*RV and for the use of 3′-PS analogues as mechanistic probes are discussed.
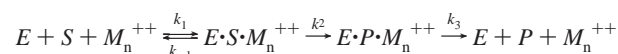
Results

Kinetic Analysis of 3′-PS Cleavage by *Eco*RV. Previous examination of 3′-PS analogue cleavage by *Eco*RV showed that specific activities were reduced by 10^4-fold or more in the presence of each of the three metals Mg^{2+}, Mn^{2+}, and Co^{2+}.[19] To provide a definitive set of kinetic constants for correlation with X-ray structures, the rate of the chemical step for cleavage of 16-mer oligodeoxynucleotides containing the GATATC target site, in the context of both unmodified and 3′-S-phosphorothiolate (3′-PS) duplex DNAs, was determined at pH 7.5 for the five divalent metals Mg^{2+}, Mn^{2+}, Co^{2+}, Zn^{2+}, and Cd^{2+} (Table 1). For native 3′O substrates, the Mn^{2+}-dependent phosphoryl transfer rate is 6-fold faster than that mediated by either Mg^{2+} or Co^{2+}. Cleavage in the presence of either Zn^{2+} or Cd^{2+} was not detected even after incubation with enzyme for 95 h. These data are in accord with previous measurements.[15,17,18,25,26] The substitution of sulfur at the 3′-leaving position produces very large decreases in catalytic rates for each of the three active

Table 1. Cleavage Rates of 3′-phosphorothiolate and Unmodified Substrates[a]

k_2 (sec^{-1}) divalent metal	3′O	3′S
Mg^{2+}	0.6 ± 06[b]	- - -[c]
Mn^{2+}	4.1 ± 0.2[b]	- - -
Co^{2+}	0.52 ± 0.08	- - -
Zn^{2+}	- - -	- - -
Cd^{2+}	- - -	- - -

[a] The kinetic scheme for duplex DNA cleavage by *Eco*RV (E) is depicted below. S and P represent the intact and cleaved duplexes, and k_2 is the rate constant for cleavage of either single strand. The 16-mer substrates studied possess the sequence 5′-GGGAAAGATATCTTGG with the cleavage site underlined. 3′O and 3′S refer to wild-type and 3′-phosphorothiolate DNAs, with the modification consisting of a sulfur substitution for oxygen at the bridging 3′-position of the center TA step of the target site. The rates of cleavage for this strand and its complement are determined from the appearance of 7-mer and 9-mer products, and are identical within experimental error.[18,26] It is well-established that the number of metal ions required for catalysis (M_n) is at least two per enzyme subunit.[4,25]

$$E + S + M_n^{++} \underset{k_{-1}}{\overset{k_1}{\rightleftharpoons}} E{\cdot}S{\cdot}M_n^{++} \overset{k2}{\longrightarrow} E{\cdot}P{\cdot}M_n^{++} \overset{k_3}{\longrightarrow} E + P + M_n^{++}$$

[b] These rates are taken from (26). [c] No observable cleavage after 95 h incubation at 37 °C.

metals. Further, none of the thiophilic metals Mn^{2+}, Zn^{2+}, or Cd^{2+} are able to provide any reconstitution of activity (Table 1).[27]

Overall Structures and Conformation of Duplex DNA Containing 3′-PS Linkages. Crystals of wild-type *Eco*RV bound to the cognate sequence GATATC containing a *3′-S*-phosphorothiolate at the scissile phosphate (3′-PS DNA) grew in a triclinic space group isomorphous with those of both the wild type/cognate DNA binary complex[12] and the ternary complex cocrystallized with Ca^{2+} ions[11] (*Eco*RV/3′O and *Eco*RV/3′O/Ca^{2+}, respectively). Crystals were cryoprotected, flash-frozen, and maintained at 100 K during data collection to prevent radiation decay. The crystals diffract to very high resolution (2.0, 1.9, and 1.6 Å for the *Eco*RV/3′S/Mg^{2+}, *Eco*RV/3′S/Mn^{2+}, and *Eco*RV/3′S/Ca^{2+} structures, respectively), and each model refined with good agreement to the diffraction data while maintaining tight stereochemical constraints (Table 2). Each structure is very similar to that of wild-type *Eco*RV bound to 3′O cognate DNA in this crystal form. Superpositions of main-chain atoms among the core DNA-binding domains of 3′O and 3′S structures (comprising 122 amino acids)[11] yield rms deviations between 0.15 and 0.3 Å, within the coordinate errors.

The very weak activity of *Eco*RV toward 3′-PS analogues permits cocrystallizations in the presence of metal ions without cleavage of the DNA. Electron density for both strands of the DNA is strong and continuous across the scissile phosphate, indicating that a pre-transition state configuration with intact duplex DNA has been trapped in each of the three structures. Refinements of the two P–S linkages were first carried out with relaxed constraints (bond energies at one-fifth of those in unmodified phosphates), and the absence of residual difference electron density in $(F_o - F_c)$ maps above 1.0 σ at the end of refinement was verified. Analysis of the refined structures shows that the average P–S bond length is 2.02 Å and the average C3′–S bond length is 1.73 Å. The P–S bond lengths are comparable to those described for small-molecule structures, which range between 1.95 and 2.1 Å;[28–30] these are longer than

(24) Szczelkun, M. D.; Connolly, B. A. *Biochemistry* **1995**, *34*, 10724.

(25) Baldwin, G. S.; Vipond, I. B.; Halford, S. E. *Biochemistry* **1995**, *34*, 705.

(26) Sam, M. D.; Perona, J. J. *J. Am. Chem. Soc.* **1999**, *121*, 1444.

(27) The Mg^{2+}-dependent cleavage of the base-analogue substrate GA<u>C</u>GTC proceeds with a rate constant $k_2 = 5.2 \times 10^{-7}$ sec^{-1} (ref 15). Because the enzyme begins to lose activity after 120 h in the reaction conditions used, this represents approximately the slowest practically measurable rate.

Table 2. Data Collection and Structure Refinement Statistics

	*Eco*RV/3′S/Mg^{2+}	*Eco*RV/3′S/Mn^{2+}	*Eco*RV/3′S/Ca^{2+}
space group	P1	P1	P1
cell dimensions			
Å	48.0 × 48.5 × 63.8	47.7 × 48.5 × 63.7	47.9 × 48.6 × 63.9
deg	97.0 × 108.9 × 106.3°	96.7 × 109.6 × 106.3°	96.9 × 108.9 × 106.8°
asymmetric unit	one dimer, one DNA duplex	one dimer, one DNA duplex	one dimer, one DNA duplex
resolution, Å	2.0 Å	1.9 Å	1.6 Å
total observations	55 892	72 080	128 582
unique observations	31 662	36 838	65 611
completeness, %	92.8 (90.5)^a	96.5 (95.0)^a	94.7 (92.8)^a
R_{merge}^{b}, %	13.1 (35.8)^a	5.3 (36.2)^a	3.7 (32.4)^a
I/σ^{c}	7.4 (2.3)^a	6.7 (2.5)^a	8.9 (3.0)^a
R_{cryst}^{d}, %	19.6 (4.9 to 2.0 Å)	21.3 (4.9 to 1.9 Å)	22.9 (4.9 to 1.6 Å)
R_{free}^{e}, %	29.0 (4.9 to 2.0 Å)	30.5 (4.9 to 1.9 Å)	28.1 (4.9 to 1.6 Å)
overall *B*-factor^f, Å^2	32.2	29.7	23.1
rms deviation − bond lengths	0.013 Å	0.013 Å	0.011 Å
rms deviation − bond angles	2.12°	2.01°	2.40°
no. water molecules	297	277	357
missing segments	subunit A 144, 154−5, subunit B 98−100, 142−6, DNA Ade-C1	subunit A 142−4, 154−5, 225, subunit B 98−101, 142−6, DNA Ade-C1, Thy-D11	subunit A 142−4, 154−8, subunit B 98−101, 142−6,228

^{a} Numbers in parentheses refer to statistics for the highest 0.1 Å resolution shell. ^{b} $R_{\text{merge}} = (\sum_h\sum_i|\langle F_h\rangle - F_{hi}|)/(\sum_h F_h)$ where $\langle F_h\rangle$ is the mean structure factor magnitude of i observations of symmetry-related reflections with Bragg index h. ^{c} I/σ, average intensity over sigma. ^{d} $R_{\text{cryst}} = (\sum_h\sum_i||F_{\text{obs}}| - |F_{\text{calc}}||)/(\sum|F_{\text{obs}}|)$ where F_{obs} and F_{calc} are the observed and calculated structure factor magnitudes. ^{e} R_{free} is calculated with removal of 2% of the data as the test set at the beginning of refinement ^{f} Overall *B*-factor is determined from a Wilson plot of the structure factor data using a low-resolution cutoff of 4.9 Å.

the 1.84 Å reported for 3′-PS single-stranded DNA bound to the Klenow fragment of *E. coli* DNA polymerase I.[23] Refinements were also performed with energy constraints on P−S bond lengths at 0 and 100% of the usual levels. In these experiments the average P−S bond lengths refined to 1.92 and 2.07 Å, respectively, with 2.07 Å being the value of the constraint. The refinement at zero constraint produced residual positive difference density behind the sulfur, suggesting that the true bond length is longer than 1.92 Å, consistent with small-molecule structures.

The introduction of the phosphorothiolate linkage into each strand of the duplex causes relatively minor perturbations to the local DNA conformation. The directly connected ribose sugar 5′ to the P−S bond is shifted by 0.5−1.0 Å in each structure, and there are some small changes in the ring pucker. Despite this shift, the thymine base of the center 5′-TA-3′ step occupies nearly the same position in unmodified and 3′S structures, and there are no alterations in conformation 3′ to the P−S bond with the exception of one subunit of *Eco*RV/3′S/Mn^{2+} (see below). Comparisons among all 3′O and 3′S structures reveal some differences in the structure of the minor-groove binding "Q-loops"—in particular, a peptide-bond flip at Gln69 and two alternative rotamers for the Asn70 side chain. However, these differences are not consistently correlated with the presence of the 3′-PS modification and sometimes also differ between the two subunits of a given structure. Flexibility of the Q-loops has been previously noted in other analyses.[11,12]

There are also some effects of the phoshorothiolate substitution on certain helical parameters for the base-pair steps in duplex DNA (Figure 2).[31,32] Calculations of the possible

rotations of adjacent base-pair steps shows that the helical twist at the center 3′-PS modified TA step is 3−8° larger than in unmodified DNA. However, there is no correlation of either the base-pair roll or tilt parameters with the presence of the sulfur. Certain translational parameters also differ: while the slide (Dy) is unaffected, values of the base-pair rise and particularly the shift (Dx) at both the center TA and adjacent AT step are correlated with the 3′-PS modification.[32] The difference in shift is approximately 0.5 Å. Thus, small structural perturbations to the duplex do arise. These appear to be of some functional significance when the modified DNA is bound in a ternary complex with *Eco*RV and divalent metal ions (see Discussion).

Structure of the *Eco*RV/3′-PS/Ca^{2+} Complex. Two calcium ions have been located in the active site of each subunit (Figure 3). One of these binds at a site near to but not directly ligating the DNA (site I). It forms inner-sphere interactions in a roughly octahedral geometry with a carboxylate oxygen atom of Asp74, the main-chain carbonyl group of Ile91, and four water molecules (Table 3). The second calcium ion is found deeper in the active site (site II), where it makes inner-sphere contacts with seven ligands: the two carboxylate oxygens of Glu45, one carboxylate oxygen of Asp74, and four water molecules. All of the inner-sphere ligands of the calcium ions are identical in the two subunits, although some of the distances are slightly altered. Also, several site I inner-sphere waters in direct contact with the DNA make somewhat different interactions in the two subunits. In subunit A, one of these waters lies within hydrogen-bonding distance of both the 3′-bridging and *pro-S* oxygens of the 3′-adjacent phosphate, while a second bridges to the *pro-S* oxygen of the scissile phosphate, a carboxylate oxygen of Asp90, and the terminal amine group of Lys92 (Figure 3a). However, in subunit B the calcium ion in site I is displaced 0.5 Å farther from the DNA relative to its position in subunit A, so that the former inner-sphere water contacts only the 3′-bridging oxygen of the 3′-adjacent phosphate, whereas the second maintains hydrogen-bonds with the scissile phosphate and with Asp90, but not with Lys92.

(28) Corbridge, D. E. C. *Studies in Inorganic Chemistry 6, Phosphorus*, 3rd ed.; Elsevier: Amsterdam, 1985; pp 38−39.

(29) Saenger, W.; Eckstein, F. *J. Am. Chem. Soc.* **1970**, *92*, 4712.

(30) (a) Frey, P. A.; Sammons, R. D. *Science* **1985**, *228*, 541. (b) Baraniak, J.; Frey, P. A. *J. Am. Chem. Soc.* **1988**, *110*, 4059. (c) Liang, C.; Allen, L. C. *J. Am. Chem. Soc.* **1987**, *109*, 6449.

(31) Lavery, R.; Sklenar, H. *J. Biomol. Struct. Dyn.* **1989**, *6*, 655.

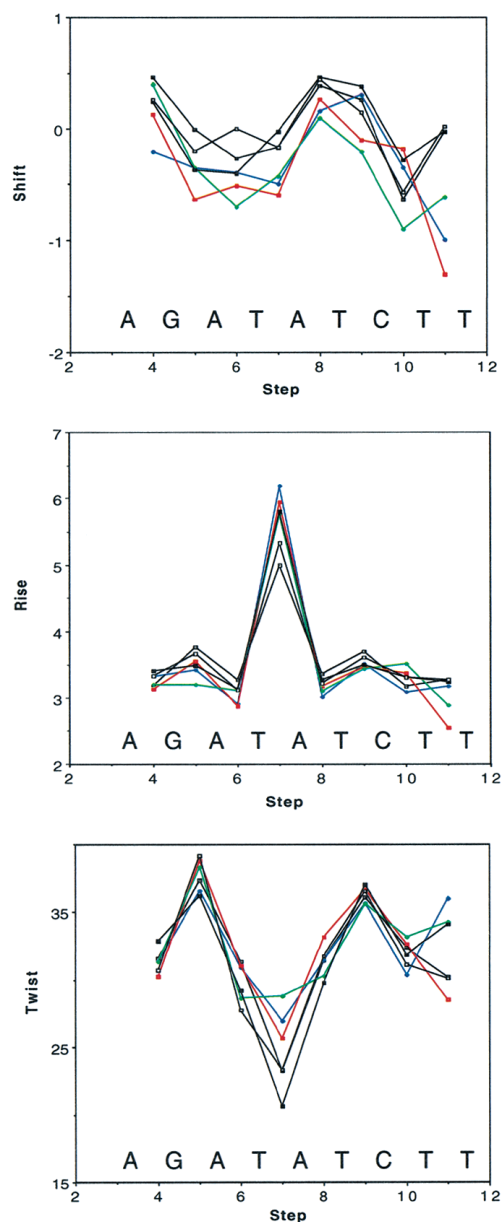(32) Dickerson, R. E. et al. *EMBO J.* **1989**, *8*, 1.

Figure 2. DNA structural parameters for *Eco*RV-DNA complexes. The color coding for each plot is red: *Eco*RV/3′S/Mg²⁺ structure, blue: *Eco*RV/3′S/Ca²⁺ structure, green: *Eco*RV/3′S/Mn²⁺ structure, filled black boxes: *Eco*RV/3′O/Ca²⁺ structure,[11] open black boxes: *Eco*RV/3′O/Mg²⁺ structure,[12] dotted black boxes: *Eco*RV/3′O structure in the absence of metal ions.[12] (Top) plot of the shift (Dx) as a function of base-pair step along the duplex DNA sequence. The identities of the base-pair steps across the GATATC target site are indicated. (Center) plot of the base-pair rise as a function of position along the DNA duplex. (Bottom) plot of the base-pair twist as a function of position along the DNA duplex.

Neither of the two calcium binding sites observed in the *Eco*RV/3′S/Ca²⁺ structure are occupied in the wild-type ternary complex cocrystallized with Ca²⁺ (*Eco*RV/3′O/Ca²⁺).[11] Instead, in the wild-type complex a single Ca²⁺ ion bound per subunit is ligated directly to the scissile phosphate, Asp90 and Asp74 (Figure 4). This site (site III, Figure 1) is also occupied by Mg²⁺, Mn²⁺, and Co²⁺ in various soaking and cocrystallization experiments.[12] In addition to the direct ligation to the scissile phosphate, an inner-sphere water molecule from this metal ion hydrogen-bonds to the 3′-oxygen. Thus, substitution of the oxygen with sulfur is sufficiently disruptive to cause the displacement of a hydrated Ca²⁺ ion from this site, even though

the local structural perturbations from the sulfur cause only very small rearrangement in the relative positions of the directly coordinating groups (Figure 4). The mobilities of the DNA and adjacent active-site residues, as judged by crystallographic B-factors, also do not differ significantly between the *Eco*RV/ 3′O/Ca²⁺ and *Eco*RV/3′S/Ca²⁺ structures.

Although the Ca²⁺ binding sites in the *Eco*RV/3′S/Ca²⁺ structure are unlike those in the wild-type complex, they do very closely resemble two Ca²⁺ binding sites found in one active site of *Eco*RV mutant T93A cocrystallized with cognate DNA and Ca²⁺ ions in an isomorphous space group (Figure 5).[14] The inner-sphere interactions with the enzyme are identical between T93A/DNA/Ca²⁺ and *Eco*RV/3′S/Ca²⁺ for the calcium ions at both sites I and II, although there are small differences in the ligated water structure. Two of the waters bound to the site II Ca²⁺ (Wats 318 and 273, Table 3) are not apparent in the T93A electron density maps, and one such water (Wat 18) ligated to the site I Ca²⁺ is similarly not evident in T93A. Also, a small difference in the conformation of Asp90 results in a long 3.1 Å contact with the site I Ca²⁺ in T93A but not in the *Eco*RV/ 3′S/Ca²⁺ structure. A final minor difference is that the water molecule bridging to the adjacent 3′-phosphate is better-positioned in T93A to make a close hydrogen bond with the *pro-S* oxygen of this moiety. The coincidence of binding site I, now found in the context of two quite different perturbations to the wild-type structure, further validates a proposed role in the catalytic mechanism (see Discussion).[14,18]

Structure of the *Eco*RV/3′-PS/Mg²⁺ Complex. Difference electron density maps, including simulated-annealing omit maps, suggest that two Mg²⁺ ions bind in each active site (Figure 6). Their positions are nearly identical to those occupied by Ca²⁺ ions in the *Eco*RV/3′S/Ca²⁺ structure. The only significant difference in the immediate active-site enzyme conformation of *Eco*RV in these two structures is a small reorientation of the Glu45 carboxylate, such that inner-sphere contacts to both oxygens in the Ca²⁺ structure are replaced with only one such contact in the Mg²⁺ structure. Because the electron density of Mg²⁺ is identical to that of a water molecule, the assignment of binding sites is necessarily somewhat less definitive than for larger Ca²⁺ ions. The Mg²⁺ ions bound in site II ligate five and six inner-sphere oxygen atoms in subunits A and B, respectively, with roughly octahedral geometry, short Mg−O distances, and B-factors of 33 and 29 Å² (Table 3). In subunit B, the Mg²⁺ occupying site I refines to a B-factor of 45 Å² with five short inner-sphere ligands, but the equivalent Mg²⁺ in subunit A appears to be less tightly bound. It ligates only four inner-sphere oxygens with one of these at 2.6 Å distance; further, the B-factor for this Mg²⁺ refines to a very high value of 71 Å². Although the short interatomic distances for the other three waters suggest that this electron density feature does represent a Mg²⁺ ion, we cannot fully exclude the possibility that a water molecule is present instead. In the case of the other three sites, the assignment of an Mg²⁺ ion can be made with confidence. In neither subunit does the hydrated Mg²⁺ ion at site I make a hydrogen-bond with the *pro-S* oxygen of the adjacent 3′-phosphate (as does hydrated Ca²⁺), although in subunit B a long 3.4 Å interaction with the 3′-bridging oxygen of this phosphate does exist.

Soaking experiments in which Mg²⁺ was introduced into crystals of the binary wild-type *Eco*RV-DNA complex in this space group have previously localized two binding sites.[12] The DNA remained uncleaved and the Mg²⁺ ions were bound in only one of the two active sites. In contrast to the *Eco*RV/3′S/
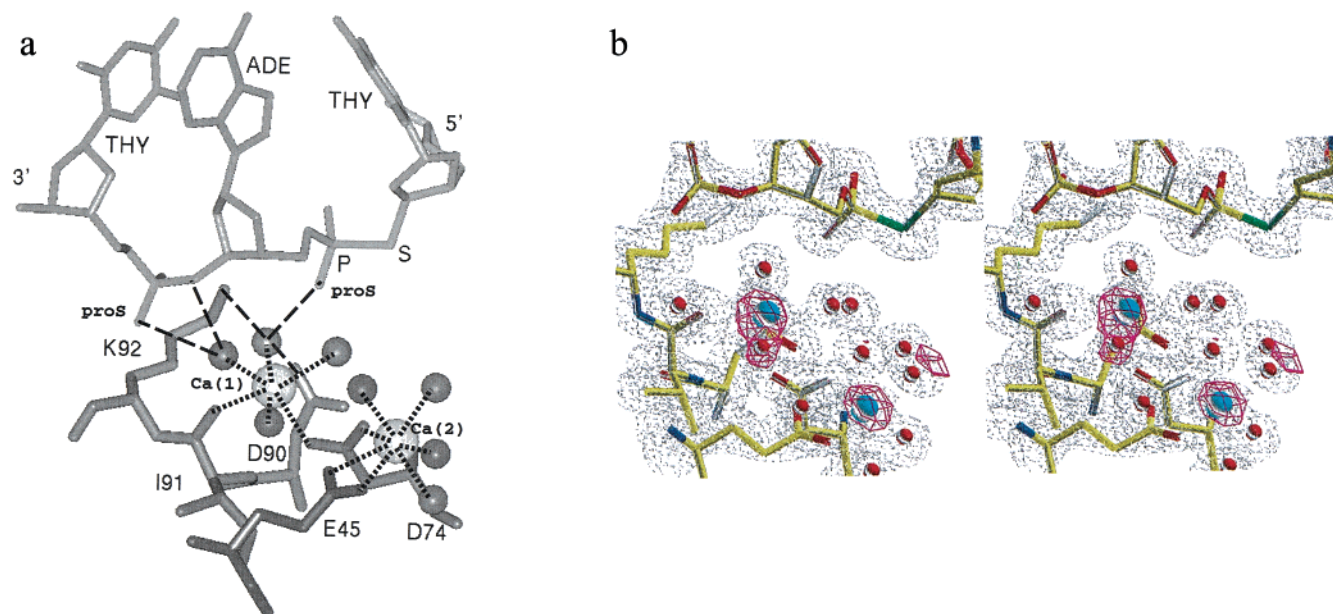
Figure 3. (a) Active-site structure in subunit A of the *Eco*RV/3′S/Ca^{2+} complex. Ca(1) and Ca(2) are labeled as in Table 3 and occupy sites I and II, respectively (see Figure 1). The position of the new P−S bond in the DNA is shown. Short dotted lines indicate inner-sphere metal ligands; dashed lines indicate hydrogen-bonding interactions. (b) Electron density maps calculated in the active site of subunit A of the *Eco*RV/3′S/Ca^{2+} complex. *Gray contours*: map calculated with coefficients $(2F_o - F_c)$, after removal of metal ions in each active site followed by a positional refinement protocol in XPLOR. The map is computed in the resolution range from 1.6 to 20 Å, with phases derived from the model with the metal ions deleted. *Red contours*: map calculated with coefficients $(F_{o,3'S-Ca} - F_{o,3'S-Mg})$ in the resolution range from 2.0 to 20.0 Å. Phases are derived from the refined *Eco*RV/3′S-DNA/Mg^{2+} model with Mg^{2+} ions removed. The density is contoured at 1.0 σ for the $(2F_o - F_c)$ map and 3.0 σ for the $(F_o - F_o)$ map. The blue spheres represent Ca^{2+} ions, and red spheres represent waters. The sulfur atom of the modified DNA is in green. The maps were drawn using O.[43]

Table 3. Metal Binding Sites

EcoRV/3′S/Mg^{2+}			EcoRV/3′S/Mn^{2+}			EcoRV/3′S/Ca^{2+}		
metal	ligand	distance(Å)	metal	ligand	distance(Å)	metal	ligand	distance(Å)
Mg^{2+} (1)	Ile91 O	2.64	Mn^{2+} (1)	Glu45 OE1	2.69	Ca^{2+} (1)	Asp74 OD2	2.40
subunit A	Asp74 OD2	2.21	subunit A	Asp74 OD2	2.18	subunit A	Ile91 O	2.43
B = 71 Å^2	Wat 152	2.33	B = 58 Å^2	Ile91 O	2.41	B = 39 Å^2	Wat 27	2.35
	Wat 15	2.18		Wat 24	1.98		Wat 350	2.44
				Wat 23	2.10		Wat 18	2.39
Mg^{2+} (2)	Asp74 OD1	2.39		Wat 127			Wat 289	2.43
subunit A	Glu45 OE2	1.98						
B = 33 Å^2	Wat 233	2.04	Mn^{2+} (2)	Glu45 OE2	2.37	Ca^{2+} (2)	Glu45 OE1	2.47
	Wat 154	2.21	subunit A	Asp74 OD1	2.83	subunit A	Glu45 OE2	2.48
	Wat 14	2.11	B = 54 Å^2	Wat 25	1.98	B = 28 Å^2	Asp74 OD1	2.62
				Wat 170	2.07		Wat 318	2.41
Mg^{2+} (3)	Glu45 OE1	2.00		Wat 243	2.14		Wat 13	2.36
subunit B	Asp74 OD1	2.08		Wat 207	2.00		Wat 7	2.39
B = 29 Å^2	Wat 86	2.17					Wat 273	2.36
	Wat 187	2.14	Mn^{2+} (3)	His71 NE2	2.18			
	Wat 90	2.03	subunit A	Wat 210	2.04	Ca^{2+} (3)	Glu45 OE1	2.42
	Wat 85	2.17	B = 42 Å^2	Wat 10	2.05	subunit B	Glu45 OE2	2.72
						B = 36 Å^2	Asp74 OD1	2.46
Mg^{2+} (4)	Asp74 OD2	2.19	Mn^{2+} (4)	His193 NE2	2.28		Wat 323	2.37
subunit B	Ile91 O	2.21	subunit A	Wat 33	2.16		Wat 324	2.32
B = 45 Å^2	Wat 91	2.13	B = 61 Å^2	Wat 128	2.08		Wat 101	2.56
	Wat 93	2.13		Wat 252	1.97		Wat 260	2.42
	Wat 253	2.09		Wat 208	2.03			
						Ca^{2+} (4)	Asp74 OD2	2.38
			Mn^{2+} (5)	His71 NE2	2.28	subunit B	Ile91 O	2.82
			subunit B	ThyC11 O2P	2.20	B = 55 Å^2	Wat 356	2.72
			B = 32 Å^2	Wat 83	2.36		Wat 285	2.44
				Wat 84	2.13		Wat 100	2.36
				Wat 185	1.94		Wat 259	2.49

Mg^{2+} structure reported here, in the *Eco*RV/3′O/Mg^{2+} complex the two Mg^{2+} ions occupy sites II and III but not site I (Figure 7).[12] Thus, as in the *Eco*RV/3′S/Ca^{2+} structure, the effect of the sulfur modification is to prevent the direct metal ligation of the scissile phosphate observed in native crystals. Inner-sphere

ligation of Asp74 and Glu45 by the site II Mg^{2+} ions are identical in the 3′S/Mg^{2+} vs 3′O/Mg^{2+} structures; differences appear only in water occupancies at the remaining sites in the octahedron. When main-chain atoms of the core active-site domains are superimposed, the site III Mg^{2+} ion observed on
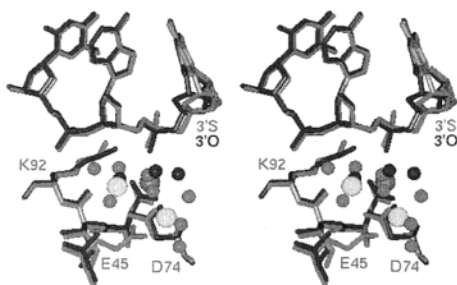
Figure 4. Superposition of the structures of *Eco*RV/3′S/Ca^{2+} (gray) and *Eco*RV/3′O/Ca^{2+} (black) in the active site of subunit A (divergent stereoview). The superposition is based on main-chain protein atoms in core regions of the DNA-binding domains (amino acids 4−9, 48−66, 71−77, 86−96, 104−137, 166−181, 188−216).[11] Large light-colored spheres represent Ca^{2+} ions in the 3′S structure (bound in sites I and II), and the large gray sphere represents the Ca^{2+} in the 3′O structure bound at site III. Water molecules ligated directly to the metals are shown as smaller spheres in gray (*Eco*RV/3′S/Ca^{2+}) and in black (*Eco*RV/3′O/Ca^{2+}).
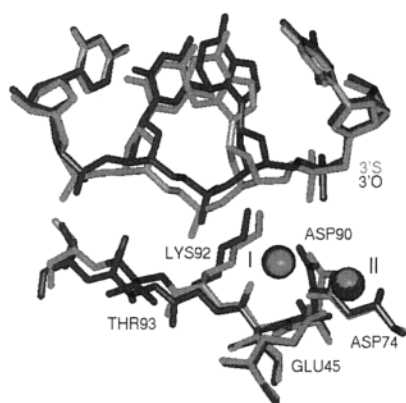

Figure 5. Superposition of the structures of *Eco*RV/3′S/Ca^{2+} (gray) and *Eco*RV T93A mutant bound to unmodified DNA and Ca^{2+} ions (black),[14] in the active site of subunit A. The superposition is performed as described in Figure 4. Thr93 in the wild-type enzyme is indicated to show the position of the mutation with respect to the active site. The Ca^{2+} ions bind in the same positions (sites I and II) in each structure (black and gray spheres).

the scissile phosphate in *Eco*RV/3′O/Mg^{2+} is found 2.1 and 2.5 Å distant from the site I Mg^{2+} atoms in subunits A and B of the *Eco*RV/3′S/Mg^{2+} structure, respectively.

The substitution of sulfur also influences the relative positions of the DNA scissile phosphate and active-site groups of the enzyme. It was found that, in the subunit of the *Eco*RV/3′O complex which binds Mg^{2+} in soaking experiments, the DNA is shifted such that the scissile phosphate is positioned approximately 1 Å more deeply into the active site. In the cocrystallized *Eco*RV/3′S/Mg^{2+} structure, the position of the DNA scissile phosphate is in an intermediate position between that adopted in the *Eco*RV/3′O and *Eco*RV/3′O/Mg^{2+} structures (Figure 7). This discrepancy between 3′O and 3′S conformations observed in the Mg^{2+} structures does not occur for Ca^{2+} ternary complexes; in that case, the sulfur substitution has no influence on the relative positions of the DNA scissile phosphates and the enzyme carboxylate groups (Figure 4).

Structure of the *Eco*RV/3′-PS/Mn^{2+} Complex. To address the structural basis for the failure of the thiophilic Mn^{2+} cation to reconstitute activity toward the 3′-phosphorothiolate analogue, the structure of *Eco*RV cocrystallized with 3′-PS and Mn^{2+} ions was determined at 1.9 Å resolution. This structure reveals that in subunit A the thiophilic Mn^{2+} ions again occupy sites I and

II in similar positions to Ca^{2+} and Mg^{2+} in the 3′S/Ca^{2+} and 3′S/Mg^{2+} structures, but do not occupy site III (Figure 8, Table 3). Thus, in *Eco*RV the 3′-phosphorothiolate linkage at the scissile phosphate excludes direct ligation of all divalent metals tested to the *pro-S* oxygen, regardless of whether the metal ion is thiophilic.[33]

Although the positions of the metal ions in sites I and II are similar in the three *Eco*RV/3′S structures, several differences appear in the Mn^{2+}-bound complex. Three Mn^{2+} ions were identified outside of the active sites, bound to His71 of each subunit and to His193 of subunit A. More importantly, no binding of Mn^{2+} can be detected in the subunit B active site in maps calculated either with coefficients (2F_o − F_c) or ($F_{o,3′S/Mn}$ − $F_{o,3′S/Mg}$) (data not shown), despite the fact that the enzyme conformation is identical to subunit A with the exception of some small movements of the Lys92 side chain (Figure 9). Superposition of the two active sites reveals that in subunit A the binding of the Mn^{2+} ions induces a shift in the 3′-PS DNA toward the enzyme of magnitude 0.4 Å to 0.8 Å. Interestingly, the shift is greatest at the position of the 3′-adjacent phosphate rather than at the scissile phosphate, perhaps because an inner-sphere water molecule of the site I Mn^{2+} ion bridges to the *pro-S* oxygen of the former. This Mn^{2+} ion is also located 0.7 Å to 1.0 Å deeper in the active site compared to the positions of the Mg^{2+} ions at site I in the *Eco*RV/3′S/Mg^{2+} structure, and is displaced by 0.6 Å relative to the positions of the site I Ca^{2+} ions in the *Eco*RV/3′S/Ca^{2+} structure. Comparisons among the three 3′-PS structures show that the position of the 3′-adjacent phosphate of the DNA, when either Mg^{2+} and Ca^{2+} is present, is identical to that of the *Eco*RV/3′S/Mn^{2+} structure in the subunit *lacking* Mn^{2+} ions. Thus, Mn^{2+} but not the other metals is able to bring about a small shift (approximately 0.8 Å) in this adjacent phosphate. In the shifted position, the site I Mn^{2+} now makes an additional (albeit long) interaction with a carboxylate oxygen of Glu45, with the side-chain of this residue undergoing a 1−2 Å reorientation to accommodate this (Figure 10). The other Glu45 carboxylate oxygen still also interacts with the Mn^{2+} ion at site II, and the remaining interactions of the site II Mn^{2+} also resemble those made by Ca^{2+} and Mg^{2+} (Table 3).

Discussion

Mechanism of Phosphoryl Transfer Inhibition by 3′*S*-Phosphorothiolates. The crystal structures of *Eco*RV endonuclease bound to duplex DNA containing 3′-PS linkages show that the sulfur substitution excludes all divalent metal binding to the scissile phosphate group (Figures 3a, 6a, and 8a). Because compensation of the incipient additional negative charge in the transition state is crucial for accelerating DNA cleavage,[34] the removal of the metal ion binding site readily explains the sharply

(33) Winkler and colleagues (ref 12) reported Mn^{2+} binding to the 90/74 site in wild-type *Eco*RV, but did not describe the ligand sphere in detail. Coordinates for this structure are not available. However, we have documented Mn^{2+} binding in the complex of the very weakly active *Eco*RV K92A mutant bound to uncleaved cognate DNA at 2.0 Å resolution, which shows no structural changes at the 90/74 site compared to the wild-type enzyme (unpublished results). In this structure, a water molecule in the inner sphere of the Mn^{2+} ion at the 90/74 site (site III in Figure 1) does hydrogen-bond to the leaving 3′O oxygen.

(34) (a) Wolfenden, R.; Ridgway, C.; Young, G. *J. Am. Chem. Soc.* **1998**, *120*, 833. (b) Blasko, A.; Bruice, T. C. *Acc. Chem. Res.* **1999**, *32*, 475. (c) Dempcy, R. O.; Bruice, T. C. *J. Am. Chem. Soc.* **1994**, *116*, 4511. (d) Westheimer, F. H. In *Phosphorus Chemistry, Developments in American Science*; Walsh, E. N., Griffith, E. J., Parry, R. W., Quin, L. D., Eds.; ACS Symposium Series; American Chemical Society: New York, 1992. (e) Dalby, K. N.; Holifelder, F.; Kirby, A. J. *J. Chem. Soc., Chem. Commun.* **1992**, 1770.
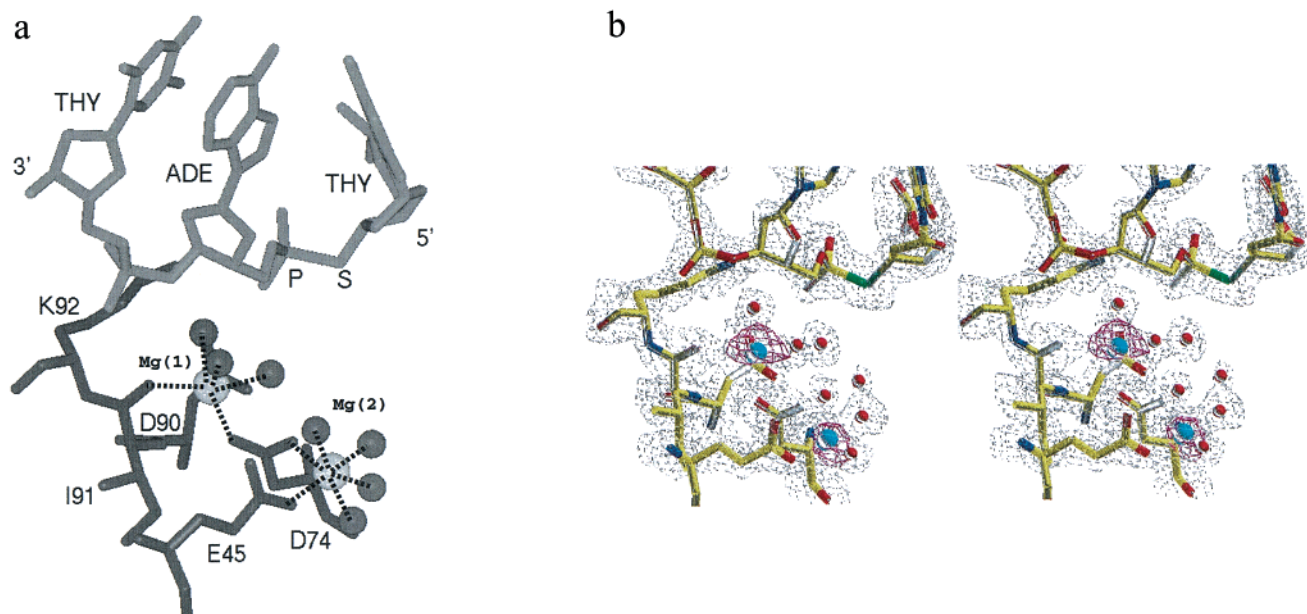
Figure 6. (a) Active-site structure in subunit B of the *Eco*RV/3′S/Mg^{2+} complex. Mg(1) and Mg(2) are labeled as in Table 3 and occupy sites I and II, respectively (see Figure 1). The position of the new P–S bond in the DNA is shown. Short dotted lines indicate inner-sphere metal ligands. (b) "Omit" electron density maps in the active site of subunit A of the *Eco*RV/3′-PS/Mg^{2+} complex. Metal ions in each active site were removed, and the resulting model was subjected to a positional refinement protocol in XPLOR. Electron density maps calculated with coefficients $(2F_o - F_c)$ (gray), and $(F_o - F_c)$ (red) are shown superimposed on the final model. Phases for these maps were derived from the model with the metal ions deleted. The maps were computed for the resolution range from 2.0 to 20 Å. The contour level of the $(2F_o - F_c)$ map is 1.0 σ, and the contour level of the $(F_o - F_c)$ map is 4 σ.
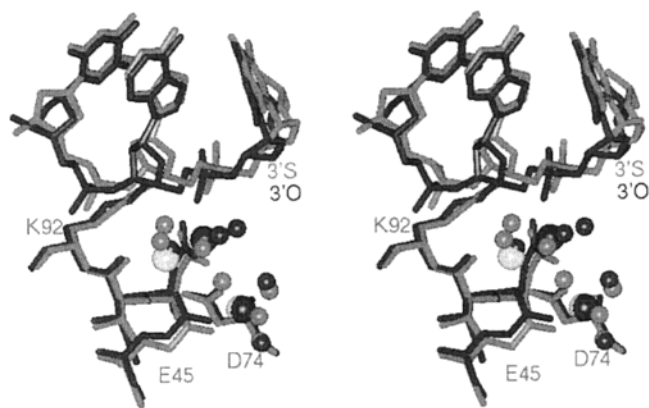

Figure 7. Superposition of the structures of *Eco*RV/3′S/Mg^{2+} (gray) and *Eco*RV/3′O/Mg^{2+} (black) in the active site of subunit B (divergent stereoview). The superposition is performed as described in Figure 4. The latter structure was visualized by soaking crystals of the binary enzyme–DNA complex in solutions containing Mg^{2+} ions, after which the DNA is not cleaved.[12] Large light-colored spheres represent Mg^{2+} ions in the 3′S structure (occupying sites I and II); black spheres represent Mg^{2+} ions in the 3′O structure (occupying sites II and III). Smaller spheres represent directly ligated waters in black (*Eco*RV/3′O/Mg^{2+}) and in gray (*Eco*RV/3′S/Mg^{2+})

decreased catalytic rates. A significant perturbation of this type is indeed expected, since sulfur is a better leaving group than oxygen and would likely increase activity in the absence of other effects.[35]

In wild-type ternary complex structures, a divalent metal ion binds directly to the *pro-S* oxygen of the scissile phosphate and ligates the leaving 3′-oxygen through an inner-sphere water molecule.[11,12] This finding from crystallography has been integrated into models for the stereochemical basis of catalysis (Figure 1a).[14] The failure of thiophilic metals to rescue activity

toward the 3′-PS analogue is consistent with leaving group protonation by an *aquo*-divalent metal ion, as compared with neutralization of the leaving anion via direct metal ligation. The 3′-5′ exonuclease domain of *E. coli* DNA polymerase I (Klenow fragment) provides an example of the alternate scenario. In this case thiophilic Mn^{2+} ions do rescue activity toward 3′-PS DNA, and the cocrystal structure with single-stranded 3′-PS DNA and Mn^{2+} ions shows direct Mn^{2+} ligation to the leaving sulfur atom (Figure 1b).[23] This provides evidence supporting a proposed two-metal mechanism in which Mg^{2+} directly interacts with the 3′-oxygen.[16a] Taken together, the combined kinetic and crystallographic investigations of Klenow fragment and *Eco*RV offer an excellent foundation for the use of 3′-PS analogues as probes of other metal-dependent phosphoryl transfer reactions. They support the conventional interpretation of *thio* effects—rescue by Mn^{2+} indicates direct contact with phosphate oxygens, whereas failure to rescue indicates a lack of such interaction (although less definitively; see below).

Other relevant structures for comparison are those of two phosphorothioates also incorporated into single-stranded DNA bound to Klenow fragment.[36] The cocrystal structure of the inactive S$_p$ isomer at the scissile phosphate revealed that Mn^{2+} binding was fully excluded, consistent with its inability to rescue catalysis. However, the *pro-S* oxygen has been shown to ligate metals directly in other X-ray structures. In contrast to the experiments with phosphorothiolates, then, these studies suggest caution in the interpretation of *thio* effects and the need to consider the possibility of metal-ion exclusion. In this case it appeared from structural analyses that the greater steric bulk of the sulfur provided a sufficient rationale for the failure of Mn^{2+} to bind and reconstitute activity.[36]

We have considered the possibility that the greater steric bulk of the sulfur might also suffice to displace the hydrated metal ion from binding to the scissile phosphate in *Eco*RV–DNA– metal ion ternary complexes. However, superpositions and

(35) (a) Milstein, S.; Fife, T. H. *J. Am. Chem. Soc.* **1967**, *89*, 5820. (b) Nakamaye, K. L.; Gish, G.; Eckstein, F. *Nucleic Acids Res.* **1988**, *16*, 9947.

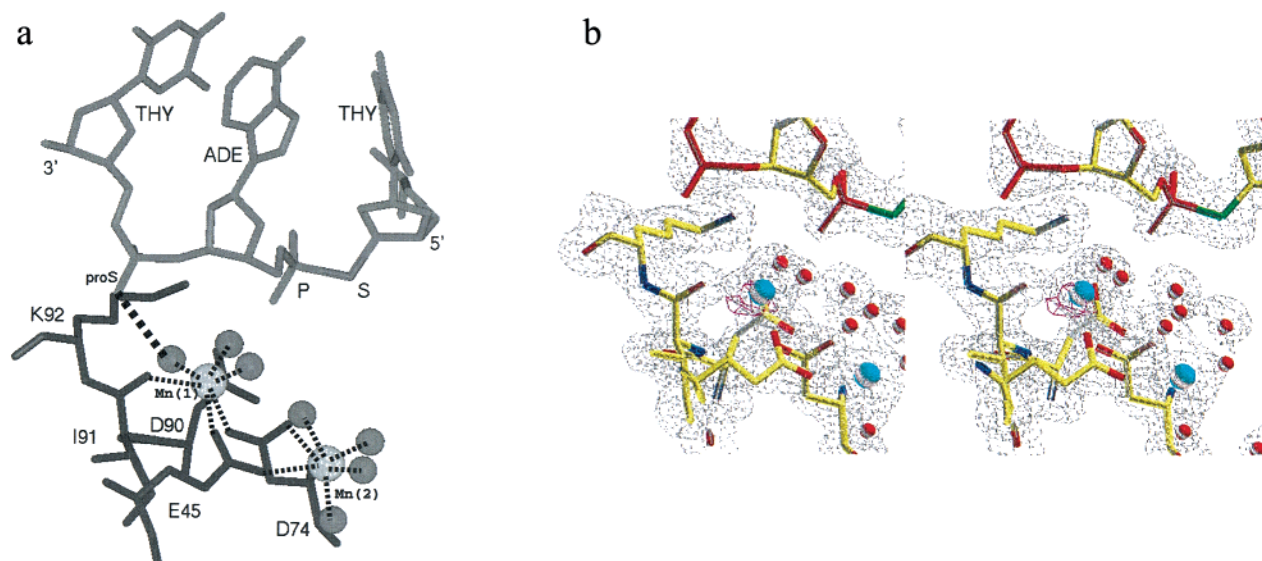(36) Brautigam, C. A.; Steitz, T. A. *J. Mol. Biol.* **1998**, *277*, 363.

Figure 8. (a) Active-site structure in subunit A of the *Eco*RV/3′S/Mn^{2+} complex. Mn(1) and Mn(2) are labeled as in Table 3 and occupy sites I and II, respectively (see Figure 1). The position of the new P−S bond in the DNA is shown. Short dotted lines indicate inner-sphere metal ligands; the heavier dashed lines indicates a hydrogen-bonding interaction. (b) Electron density maps calculated in the active site of subunit A of the *Eco*RV/3′S/Mn^{2+} complex. *Gray contours*: map calculated and displayed as described in Figure 3b, for the resolution range 1.9 to 20.0 Å. *Red contours*: map calculated with coefficients $(F_{o,3'S-Mn} - F_{o,3'S-Mg})$ in the resolution range from 2.0 to 20.0 Å. Phases are derived from the refined *Eco*RV/3′S-DNA/Mg^{2+} model with Mg^{2+} ions removed. At the 3.0 σ level this map shows a peak at the position of the site I metal in the final refined structure, but not at the position of the site II metal. The appearance of only one of the two metals may be a consequence of some non-isomorphism between the *Eco*RV/3′S/Mn^{2+} and *Eco*RV/3′S/Mg^{2+} crystals (R_{cross} of approximately 25%), and the higher *B*-factors of the Mn^{2+} ions.
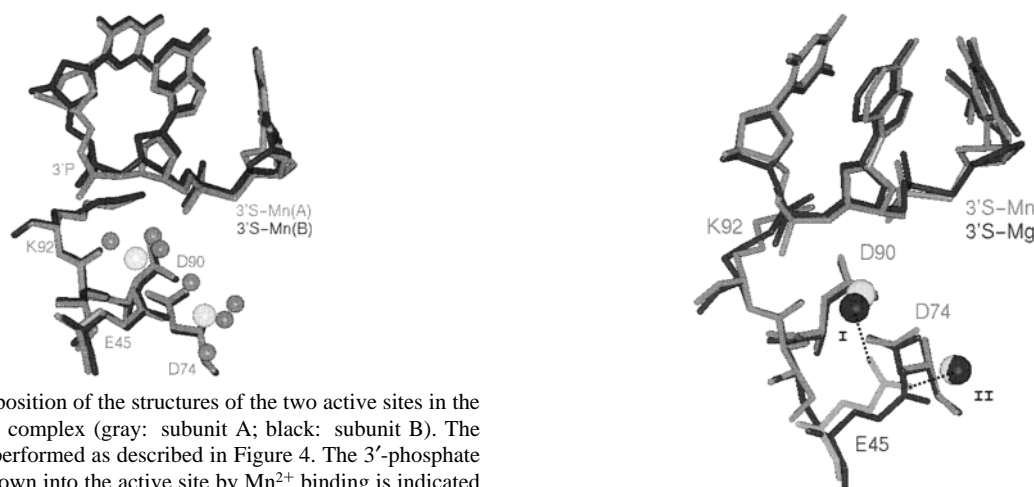

Figure 9. Superposition of the structures of the two active sites in the *Eco*RV/3′S/Mn^{2+} complex (gray: subunit A; black: subunit B). The superposition is performed as described in Figure 4. The 3′-phosphate which is pulled down into the active site by Mn^{2+} binding is indicated (3′P). Large light-colored spheres represent Mn^{2+} ions, and gray spheres represent direct water ligands to the metals.

visualization of van der Waals surfaces of the enzyme−DNA interfaces suggest that for each structure the inner-sphere water molecule bridging to the 3′O in the native structure should still be able to be accommodated. Another rationale for the exclusion of metal-ion binding to the scissile phosphate might be an alteration in the charge distribution of this group, owing to the sulfur substitution. For example, in the case of phosphorothioates, it is known that the sulfur will carry more of the negative charge—leaving the oxygen relatively electron-deficient and thus less capable of compensating the positively charged cation.[30] However, ab initio calculations for model compounds containing phosphorothiolate linkages show that the bridging sulfur does not withdraw electron density from the nonbridging phosphate oxygens (K. Kahn, personal communication). What appears more plausible is that exclusion of the hydrated metal from the scissile phosphate is instead driven by the greater hydrophobicity of sulfur. Sulfur forms much weaker hydrogen bonds than does oxygen, and this should produce a less stable interaction with

Figure 10. Superposition of *Eco*RV/3′S/Mn^{2+} (gray) and *Eco*RV/3′S/Mg^{2+} (black) in the active site of subunit A of each structure. The superposition is performed as described in Figure 4. Light gray and black spheres indicate the divalent Mg^{2+} and Mn^{2+} cations in the respective active sites. Glu45 in the *Eco*RV/3′S/Mn^{2+} structure is shown making interactions with both site I and site II metals (dotted lines).

the inner-sphere water molecule—perhaps sufficiently less stable to exclude binding of the hydrated metal. In *Eco*RV, the existence of the adjacent site I (Figure 1a) provides an alternative position for the hydrated metal ion to bind. Possibly, site III might otherwise have been occupied; that is, enzyme binding could be preferred over retention of complete octahedral water coordination in solution, even with the relatively disfavored sulfur interaction with one of the inner-sphere waters. This leaves some ambiguity with respect to whether the metal−water−3′O interaction might be similarly disrupted by sulfur in other enzymes. However, this study nonetheless establishes that the mechanism of inhibition by phosphorothiolates can differ depending upon the enzyme in question, reflecting underlying differences in the enzyme mechanisms themselves.

Metal-Dependent Binding Equilibria of the 3′-*S*-Phosphorothiolate. Gel retardation and filter-binding experiments have suggested that *Eco*RV does not bind specifically to the 3′-PS analogue.[7,24] This interpretation was based on the observation of multiple bands in gel shift experiments using 33-mer oligonucleotides and on the failure of added Mg^{2+} to resolve the bands into a single site-specific complex.[24] Further, only 4-fold improved binding affinity was detected by including Mg^{2+} in filter-binding assays, compared with measurements made in the absence of metal.[7] By contrast, the inclusion of Ca^{2+} improved the binding affinity by 700-fold.[7] The conclusions from studying the 3′-PS analogue were generalized − it was proposed both that Mg^{2+} does not improve *Eco*RV binding affinity and that the inactive Ca^{2+} cofactor is a poor model for Mg^{2+}.[7] However, other studies demonstrated at least 100-fold improved Mg^{2+}-dependent binding to active base-analogue substrates (and no change in the binding constant for nonspecific DNA), compared with binding measurements made in the absence of divalent metals.[6] Therefore, Mg^{2+} can improve the sequence specificity of binding. Moreover, these studies also showed that Mg^{2+} and Ca^{2+} have quantitatively similar effects on affinity and specificity.[6,15] It thus appeared that some structural perturbation in the phosphorothiolate complexes with *Eco*RV was responsible for the different behaviors, and that this sulfur-substituted duplex might be a poor mimic of native duplex DNA.

The cocrystal structures of *Eco*RV/3′S/Mg^{2+} and *Eco*RV/3′S/Ca^{2+} now provide the opportunity to directly examine the structural basis for the differential effects on binding affinity brought about by Mg^{2+} versus Ca^{2+}. In each subunit of the complex, the structures show that the DNA-proximal binding site (site I) is better-formed for Ca^{2+} than for Mg^{2+} (Table 3). This is most evident in the decreased interactions of the site I Mg^{2+} ions with the adjacent 3′-phosphate groups of the DNA (Figures 3a, 6a, Table 3). The average mobilities of the Mg^{2+} ions in this site are also higher than those of the Ca^{2+} ions. Analysis of the structures suggests that both the larger size of the hydrated Ca^{2+} ion and an apparent greater tolerance to accommodate a distorted ligand sphere contribute to its ability to make improved interactions and thus to increase the DNA binding affinity of *Eco*RV. By contrast, while Mg^{2+} significantly improves affinity in the context of nondisruptive base-analogue substrates, even the relatively small perturbations caused by the 3′S substitution are sufficient to greatly attenuate this. The comparison of these ternary complexes offers a vivid example of the exquisite sensitivity of metal ion binding to the protein environment and shows in detail how different metals can vary in their tolerance for small alterations in local structure. The complexes formed by *Eco*RV with 3′-PS DNA are clearly specific in character, since the DNA is sharply bent at the center TA step as in the wild-type complex (*Eco*RV is known not to bend nonspecific DNA).[10,13a] The 3′-phosphorothiolate substitution is indeed revealed not to be strongly perturbing when present in both strands of duplex DNA (Figure 2). However, introducing a 3′-PS modified DNA into a complex with both protein and divalent metal ions increases the potential for even small structural perturbations to have significant influence on function—and in a manner which differs depending upon which metal ion is present at the macromolecular interface.

Enzymatic Mechanism of *Eco*RV Endonuclease. The three crystal structures reported here provide some additional insight into the structural mechanism of metal-dependent phosphoryl transfer catalyzed by *Eco*RV. It is well-established from kinetic studies that at least two metal ions per subunit are required for catalysis.[4,25] Furthermore, numerous crystal structures of wild-type and modified complexes with different divalent metal ions have localized three distinct positions for metal binding within the immediate confines of the active site.[11−15] On the basis of this information, and also by analogy with metal-dependent DNA hydrolysis mechanisms in other enzymes, it appears very likely that the metal ions themselves play key roles in accelerating catalysis. What has not yet been clearly established is the precise configuration of the enzyme active site, DNA, and metal ions in the pre-transition state where hydroxide ion is poised to attack at phosphorus.

An early model in which the adjacent 3′-phosphate functions as the catalytic base now appears highly unlikely in view of the high pH-optimum (pH 8.5) for the chemical step in catalysis.[18] Other suggestions invoke conformational rearrangements in the DNA, relative to what is observed in all uncleaved crystal structures.[4,10,17] Such rearrangements are necessary for two-metal catalytic models analogous to those proposed for the 3′-5′ exonuclease of DNA polymerase I and for alkaline phosphatase, because the metal ions at sites II and III are positioned along an axis perpendicular rather than parallel to the direction of nucleophilic attack (Figure 1a). Recently, we have proposed a three-metal ion mechanism, based on the finding of the new divalent metal site I in the ternary complex of *Eco*RV mutant T93A bound to cognate DNA and Ca^{2+} ions.[14] Both sites I and II are occupied by Ca^{2+} in this structure, and the structural rearrangements in the active site compared to that in wild-type are relatively small. Moreover, the T93A mutant retains high activity and a pH-rate profile nearly identical to the wild-type enzyme.[18] It was straightforward to model the apparently missing metal at site III into this structure, and then to create an energy-minimized three-metal model for a pre-transition state configuration requiring little further movement in either the DNA or the enzyme (Figure 1a).[14] The *Eco*RV/3′S crystal structures reported here now permit some further insight into the merits and deficits of this model.

The occupancy of divalent metal sites in the three *Eco*RV/3′S structures is independent of the nature of the metal ion. In each case sites I and II are occupied and site III is unoccupied. The only exception to this is for one subunit of the *Eco*RV/3′S/Mn^{2+} structure, in which we have been unable to identify any bound metals. Thus, these structures show that site I, which had previously been bound only by the catalytically inactive Ca^{2+} ion in the T93A structure, can also be filled by the active metals Mn^{2+} and Mg^{2+}. The occupancy of site I by both active and inactive metals, and in the context of two different active-site perturbations, provides good support for the proposal that it plays an important role in catalysis.[14,18] On the basis of the T93A structure, it appeared that an inner-sphere water molecule bound to this metal could be the source of the hydroxide ion required for nucleophilic attack and that the pK_a of this water might be further lowered by the presence of the adjacent positively charged Lys92 (Figure 1a).[14] Examination of the *Eco*RV/3′S structures reveals that an inner-sphere water molecule of both Ca^{2+} and Mg^{2+} occupies a nearly identical position. Because the site I Mn^{2+} binds slightly more deeply in the active site, the equivalent water in this structure is shifted away from an in-line position with respect to the required direction of attack on the scissile phosphate. However, a small DNA reorientation, as suggested on the basis of the T93A structure, would nevertheless produce an identical configuration for the hydrated site I metal in all three of the 3′S structures.

In the modeled, energy-minimized pre-transition state conformation where all three sites are occupied, the metals in sites

I and III adjacent to the DNA are 4.2 Å apart, a distance very similar to the 3.9 Å separation between metal sites in the two-metal mechanism proposed for the 3′-5′ exonuclease of DNA polymerase I and for alkaline phosphatase.[16] Despite this agreement a weakness of the *Eco*RV three-metal model, which is now reinforced by the 3′S structures, is that simultaneous metal occupancy in these two sites has not been experimentally observed. Indeed, some ambiguity exists with respect to assessing whether sites I and III represent distinct positions capable of being simultaneously occupied. Comparisons among different pairs of structures in which either site I or site III is occupied show that the estimated separation between the sites varies depending upon whether the superposition is carried out based on DNA or on protein active-site groups. The separation varies between 2.1 and 3.6 Å in different pairwise comparisons. The *P*1 lattice in which all metal sites have been located does not support catalytic activity of the crystalline enzyme, and we have previously suggested that small required movements are disallowed by lattice forces and that these movements are required for simultaneous occupancy of all three metal sites.[11,14] However, the consistent observation of occupancy of either site I or site III, but not both, demands continued consideration of an alternative possibility: that metal binding to these two positions is mutually exclusive. If this is indeed the case, then some substantial rearrangement of the local DNA conformation at the scissile phosphate (as previously suggested[4,10,17] but not yet observed in the crystal structure of a pre-transition state complex with uncleaved DNA) will be needed for a two-metal mechanism in which both metals bind the DNA.

In conclusion, while the three-metal model is consistent with all available biochemical information on *Eco*RV, this consistency can only be considered as a necessary but not a sufficient basis for a "proof" of the mechanism. Establishing the structural basis for DNA cleavage beyond a reasonable doubt requires visualization of essential catalytic elements within the confines of a single high-resolution crystal structure of a ternary complex. Clearly this elusive goal is yet to be attained.

Experimental Section

Purification of Enzyme and DNA Substrates. Wild type *Eco*RV endonuclease was overexpressed in *E. coli* and purified by chromatography on phosphocellulose and blue sepharose resins, as described.[11] For kinetic analysis, purified enzyme preparations were dialyzed into 10% (v/v) glycerol, 0.4 M NaCl, 20 mM potassium phosphate (pH 7.3), and 1 mM DTT, followed by concentration to approximately 1.0 mg/mL in an Amicon ultrafiltration cell. Small aliquots were then flash-frozen and stored at −70 °C.[18] Enzyme used for crystallization trials was stored as an ammonium sulfate precipitate at 4 °C.[11] Unmodified DNA substrates used in kinetics were purchased from Integrated DNA Technologies, Inc. and were purified on a Rainin PureDNA HPLC column developed in a gradient of TEAA/acetonitrile. Detritylation was performed on the column.[37]

Oligonucleotides containing a 3′-*S*-phosphorothiolate linkage were produced using a 3′-thiothymidine phosphoramidite, as previously described.[19,24,38] For crystallizations the self-complementary sequence 5′-AAAGAT*s*ATCTT was synthesized. Kinetic analysis was performed with the non-self-complementary 16-mer oligodeoxynucleotide 5′-GGGAAAGAT*s*ATCTTGG; both this strand and its complement were synthesized with the modified linkage. After synthesis, each of the three 3′S DNAs were lyophilized from TEAA/acetonitrile buffers containing

a small quantity of DTT to protect the P−S bond. The modified oligomers were then dissolved in water and stored at −20 °C prior to use in crystallization or kinetic assays. The purity of the 3′-*S*-phosphorothiolates was confirmed by analytical reverse-phase (C-18) HPLC.

Single-Turnover Cleavage Assays. Both modified and unmodified 16-mer DNA duplex substrates and their complements were 5′-end-labeled with [γ-^{32}P]ATP, annealed together, and purified as described.[15] Single-turnover reactions in the presence of 10 mM Mn^{2+}, Mg^{2+}, Co^{2+}, Cd^{2+}, or Zn^{2+} were carried out with 200 nM purified enzyme, 50 nM DNA at 37 °C in an assay buffer containing 50 mM Hepes (pH 7.5), 100 mM NaCl, 200 μg/mL BSA, and 1 mM tris(2-carboxyethyl)-phosphine. Very rapid reactions were carried out in a rapid-quench instrument (Kintek RQF-3), with the enzyme and DNA kept in separate syringes and divalent metal ions present in each syringe, ensuring the fastest cleavage rates.[15] All reactions were quenched with a solution containing 4 M urea and 75 mM EDTA. Aliquots (10 μL) from each timepoint were then mixed with an additional 8−10 μL of quench solution containing bromphenol blue dye, and separated on 8 M urea 20% polyacrylamide gels, followed by visualization via autoradiography on the Molecular Dynamics Storm840 PhosphorImager. Rate constants were determined by fitting the data to a first-order exponential. Data were plotted using the program *Kaleidagraph*.

Crystallization and X-ray Structure Determinations. DNA for cocrystallizations was brought to a concentration of 10 mg/mL in 50 mM Tris (pH 7.5), 1mM EDTA. *Eco*RV in 10 mM HEPES (pH 7.5), 250 mM NaCl, 1 mM EDTA, 0.1 mM DTT, and the DNA oligonucleotides were mixed to give a final concentration of 10 mg/mL *Eco*RV and 1.5-fold molar excess of DNA (1.0 mg/mL). One microliter of the protein−DNA complex was mixed with one microliter of a solution containing 100 mM HEPES (pH 7.5), 150 mM NaCl, 10−15% PEG 4K (Fluka) and either 50 mM $MgCl_2$, $MnCl_2$, or $CaCl_2$ on a siliconized coverslip and placed over a well containing the same solution. Crystals appear after 1−5 days at 17 °C. Diffraction data was collected using a Rigaku rotating copper anode X-ray generator and Raxis II detector (Mg^{2+} structure) or at SSRL beamline 7−1 at wavelength 1.05 Å on a Mar image plate detector (Mn^{2+} and Ca^{2+} structures). All crystals were cryoprotected with a solution of 25% PEG 4K, 100 mM HEPES (pH 7.5), 150 mM NaCl, 30% glycerol, and flash-frozen in a stream of nitrogen gas at 100 K. This temperature was maintained throughout data collection. The data were processed and scaled with MOSFLM and SCALA (CCP4). Each structure was phased using the previously determined *Eco*RV-DNA cocrystal structure solved in space group *P*1 (*Eco*RV/3′O)[12] with all solvent molecules removed from the initial model. Structure determinations consisted of 8−14 rounds of model rebuilding iterated with rigid-body, positional, individual *B*-factor and simulated annealing refinement, and were performed with the program XPLOR.[39] Model-building utilized the programs CHAIN[40] and LORE.[41] Parameters for the DNA used in refinement were those recently described.[42] Duplex DNA helical parameters were analyzed with the program CURVES.[31]

(37) Aggarwal, A. K. *Methods: A Companion to Methods in Enzymology* **1990**, *1*, 83.
(38) Cosstick, R.; Vyle, J. S. *Tetrahedron Lett.* **1989**, *30*, 4693.

(39) Brunger, A. T.; Kuriyan, J.; Karplus, M. *Science* **1987**, *235*, 458.
(40) Sack, J. S. *J. Mol. Graphics* **1988**, *6*, 224.
(41) Finzel, B. C. *Acta Crystallogr., Sect. D.* **1995**, *51*, 450.
(42) Parkinson, G.; Vojtechovsky, J.; Clowney, L.; Brunger, A. T.; Berman, H. *Acta Crystallogr.. Sect. D* **1996**, *52*, 57.
(43) Jones, T. A.; Zou, J. Y.; Cowan, S. W.; Kjeldgaard, M. *Acta Crystallogr., Sect. A* **1991**, *47*, 110.